nature nanotechnology

SUPPLEMENTARY INFORMATION

DOI: 10.1038/NNANO.2014.15

An antidamping spin–orbit torque originating from the Berry curvature

H. Kurebayashi, Jairo Sinova, D. Fang, A. C. Irvine, T. D. Skinner, J. Wunderlich, V. Novák, R. P. Campion, B. L. Gallagher, E. K. Vehstedt, L. P. Zârbo, K. Výborný, A. J. Ferguson, T. Jungwirth

1. FMR linewidth analysis and sample parameters

We use the phenomenological Landau-Lifshitz-Gilbert (LLG) equation to describe the spin-orbit-induced magnetisation dynamics in our (Ga,Mn)As micro-bars:

$$\frac{d\mathbf{M}}{dt} = -\gamma \mathbf{M} \times (\mathbf{H} + \delta\mathbf{H}) + \frac{\alpha_G}{M_s}\left(\mathbf{M} \times \frac{d\mathbf{M}}{dt}\right) \tag{S1}$$

Here, α_G and M_s are the dimensionless Gilbert damping constant and the saturation magnetisation respectively. The gyromagnetic factor is given by $\gamma = ge/2m_0$ with e the elementary charge and m_0 the electron mass. The first term describes precession of the magnetisation $\mathbf{M}$ around the total static magnetic field $\mathbf{H}$, which includes both magneto-crystalline anisotropy fields and the externally-applied field. Relaxation towards the equilibrium direction is expressed by the second term. When $\mathbf{M}$ is resonantly driven, in our

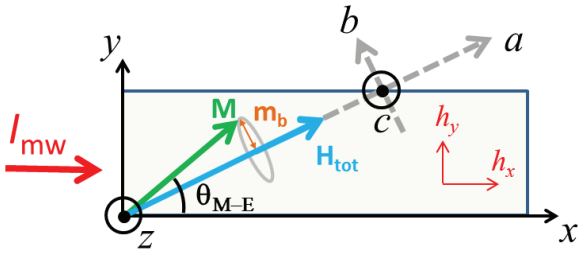

FIG. S1: The co-ordinate systems used. These are either defined with respect to the current direction (in the case of the spin orbit field) or with respect to the magnetisation (in the derivation of the rectification voltage).

case by the SO-torques included as the third term in the equation, it undergoes steady-state precession around the **H** direction. The current induced field is given by $\delta\mathbf{H}$.

We assume a small precession angle, such that the magnetisation dynamics is within the linear excitation regime, hence we can write $\mathbf{M} = (M_s, m_b e^{i\omega t}, m_c e^{i\omega t})$ within the right-hand coordinate system defined by the equilibrium orientation of **M** (shown in Supplementary Fig. S1). In this coordinate system $\delta\mathbf{H}$ can be given by the following, where $\theta_{\mathbf{M-E}}$ is the angle between **M** and the current direction.

$$\delta\mathbf{H} = \begin{pmatrix} h_x \cos\theta_{\mathbf{M-E}} + h_y \sin\theta_{\mathbf{M-E}} \\ -h_x \sin\theta_{\mathbf{M-E}} + h_y \cos\theta_{\mathbf{M-E}} \\ h_z \end{pmatrix} e^{i\omega t}, \tag{S2}$$

Solving the LLG equation to first order, the expression for m_b can be found as:

$$m_b = -\frac{[i(\omega/\gamma)h_z + (H_0 + H_1 + i\Delta H)(-h_x \sin\theta_{\mathbf{M-E}} + h_y \cos\theta_{\mathbf{M-E}})]M_\mathrm{s}}{(\omega/\gamma)^2 - (H_0 + H_1 + i\Delta H)(H_0 + H_2 + i\Delta H)} \tag{S3}$$

where $\Delta H = \alpha\omega/\gamma$ and H_1 and H_2 contain magnetic anisotropy terms:

$$H_1 = M_s - H_{2\perp} + H_{2\parallel}\cos^2\left(\varphi + \frac{\pi}{4}\right) + \frac{1}{4}H_{4\parallel}(3 + \cos 4\varphi) \tag{S4}$$

$$H_2 = H_{4\parallel}\cos 4\varphi - H_{2\parallel}\sin 2\varphi, \tag{S5}$$

$H_{2\perp}$, $H_{2\parallel}$ and $H_{4\parallel}$ represent the out-of-plane uniaxial, in-plane uniaxial and in-plane biaxial anisotropy respectively, and φ is the angle between the magnetisation vector **M** and the [100] crystallographic axis. For in-plane equilibrium orientation of **M**, only the alternating in-plane angle ($\sim\mathrm{m}_b(\mathrm{t})/\mathrm{M}_s$) will lead to a rectification voltage, and we can neglect the out-of-plane component of the precession. The magnetisation precession causes a time-varying resistance change originating in the anisotropic magnetoresistance (AMR): $R(t) = R_0 - \Delta R\cos^2(\theta_{\mathbf{M-E}} + m_b(t)/M_s)$. This, together with a microwave current at the same frequency, produces a voltage, $V(t) = I\cos(\omega t)\cdot R(t)$, and we measured the dc component which is given by $V_\mathrm{dc} = (I\Delta R m_b/2M_s)\sin 2\theta_{\mathbf{M-E}}$. Using Eq. (S3) with the above approximation and focusing on the real components, we can find the dc component as:

$$\mathrm{Re}\{V_\mathrm{dc}\} = V_\mathrm{sym}\frac{\Delta H^2}{(H_0 - H_\mathrm{res})^2 + \Delta H^2} + V_\mathrm{asy}\frac{\Delta H(H_0 - H_\mathrm{res})}{(H_0 - H_\mathrm{res})^2 + \Delta H^2} \tag{S6}$$

$$V_\mathrm{sym}(\theta_{\mathbf{M-E}}) = \frac{I\Delta R\omega}{2\gamma\Delta H(2H_\mathrm{res} + H_1 + H_2)}\sin(2\theta_{\mathbf{M-E}})h_z \tag{S7}$$

$$V_\mathrm{asy}(\theta_{\mathbf{M-E}}) = \frac{I\Delta R(H_\mathrm{res} + H_1)}{2\Delta H(2H_\mathrm{res} + H_1 + H_2)}\sin(2\theta_{\mathbf{M-E}})(-h_x \sin\theta_{\mathbf{M-E}} + h_y \cos\theta_{\mathbf{M-E}}) \tag{S8}$$

We used these equations to quantify h_x, h_y and h_z from the in-plane angle dependence of $V_{\rm dc}$. Each FMR trace was first fit by a function with symmetric and anti-symmetric Lorentzians and both components are analysed by $V_{\rm sym}(\theta_{\mathbf{M-E}})$ and $V_{\rm asy}(\theta_{\mathbf{M-E}})$. In Supplementary table I we list experimental measurements of the magnetisation independent in-plane and magnetisation dependent out-of-plane spin-orbit fields for our set of 8 samples.

In Supplementary table II, we give the uniaxial (H_u) (along [1-10]) and cubic (H_c) anisotropies; $\mu_0 M_{\rm eff}$ and the linewidth (at a frequency of 11 GHz) for each of our 8 samples, extracted from the angle-dependent FMR measurements. In addition, we show the sample resistances and AMRs.

Sample	1	2	3	4	5	6	7	8
Direction	[100]	[100]	[010]	[010]	[110]	[110]	[1-10]	[1-10]
$\mu_0 h_x$ (μT)	-49	-91	132	96	2	2	<1	<1
$\mu_0 h_y$ (μT)	-17	-15	-49	-30	127	120	-201	-145
$\mu_0 h_z - \sin\theta_{\mathbf{M-E}}$ (μT)	51	95	-122	-107	4	6	8	5
$\mu_0 h_z - \cos\theta_{\mathbf{M-E}}$ (μT)	20	41	19	42	161	203	-127	-86
$\mu_0 h_z$ - const. (μT)	-10	13	-23	25	27	<1	27	2

TABLE I: Amplitudes of the spin-orbit effective fields for different directions and symmetries.

Sample	1	2	3	4	5	6	7	8
Direction	[100]	[100]	[010]	[010]	[110]	[110]	[1-10]	[1-10]
$\mu_0 H_c$ (mT)	59	66	61	65	62	62	60	58
$\mu_0 H_u$ (mT)	59	43	45	68	40	38	51	65
$\mu_0 M_{\text{eff}}$ (mT)	429	411	437	360	404	402	350	368
$\mu_0 \Delta H$ (mT)	7.1	7.4	8.2	6.8	9.4	8.8	7.5	6.9
AMR (Ω)	45	44	44	45	151	154	140	129
R (kΩ)	11.3	11.3	11.3	11.3	11.4	11.4	11.5	10.7

TABLE II: Magnetic anisotropy and transport parameters in the studied devices.

2. Relative phase of current and current induced field

Our analysis of the spin-orbit torque depends on the current generated effective field acting on the magnetization being in phase with the current itself. From a physical perspective we expect this to be the case in our experimental geometry, since the conductivity of (Ga,Mn)As at microwave frequencies can be still safely considered to have a dominant real part. This can be seen assuming the Drude model, $\sigma = \sigma_0/(1 + i\omega\tau)$, and taking $\tau = \hbar/\Gamma$ with the Born approximation $\Gamma = 25$ meV as the upper bound for the lifetime for which we get $\omega\tau < 2.5 \times 10^{-4}$ at 10 GHz.

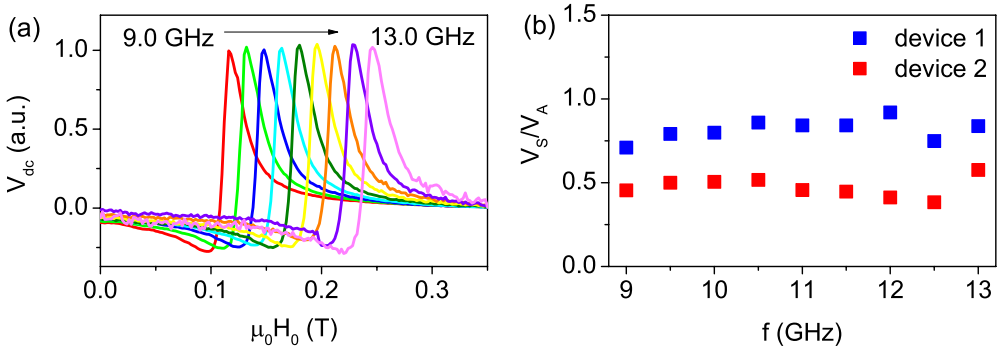

FIG. S2: Frequency dependence. (a) The rectification voltage showing FMR for several different frequencies of the microwave current. Due to the frequency dependent attenuation on the cable, the amplitude of the signals are scaled to enable comparison. (b) The ratio of symmetric to anti-symmetric components of the FMR signal, shown for two separate devices.

In light of a recent experiment by Harder *et al.*[1] we should consider the possibility that some technicality in the microwave set-up may lead to a phase shift between the current and current induced field. In that experiment, FMR is driven in a ferromagnetic microbar by the Oersted field from a short-circuited waveguide. A rectification voltage is also seen, due to a microwave current induced in the micro-bar by inductive or capacitive coupling to the current carrying waveguide. While the Oersted field driving FMR is surely in phase with the microwave current in the waveguide, it has a frequency-dependent phase (due to the coupling reactance) with respect to the coupled current in the micro-bar. As a result, as frequency is swept over a modest range (5 - 5.6 GHz), the ratio of symmetric to antisymmetric Lorentzians in the rectification signal changes by 3 orders of magnitude. We repeated our measurements for a pair of devices over a wider frequency range (9 - 13 GHz) and observe no change in this ratio, within experimental error (see Supplementary Fig. S2). We therefore exclude the presence of a frequency dependent phase shift between current and magnetic field.

3. Theory of Intrinsic Spin-Orbit Torque

The dynamical interaction of the magnetization originating from localized moments arising from the d-electrons and the delocalized hole carriers in (Ga,Mn)As gives rise to an

effective current-induced field $\delta\mathbf{H}$. The magnetization dynamics is then described by the Landau-Lifshitz-Gilbert equation (S1). The current induced field in this equation is given by

$$\mu_0\mathbf{h} = -\frac{J_{\rm ex}}{g\mu_{\rm B}}\mathbf{S}, \tag{S9}$$

where $\mu_{\rm B}$ is the Bohr magneton, $g = 2$ corresponds to the localized d-electrons in (Ga,Mn)As, and $J_{\rm ex} = 55$ meV nm^3 is the antiferromagnetic kinetic-exchange coupling between the localized d-electrons and the valence band holes, termed J_{pd}. $\delta\mathbf{s}$ is the current induced non-equilibrium spin densities. We model the carriers in these systems by a Hamiltonian with a kinetic exchange coupling term $H = H_{\rm GaAs} + H_{\rm ex}$, where $H_{\rm ex} = J_{\rm ex}c_{\rm Mn}S_{\rm Mn}\hat{\mathbf{M}}\cdot\mathbf{s}$, $H_{\rm GaAs}$ refers to the 4-band strained Kohn-Luttinger Hamiltonian for the hole systems of GaAs (see below), $\mathbf{s}$ is the 4×4 spin operator for the holes described by the four-band Kohn-Luttinger model, $S_{\rm Mn} = 5/2$, and $c_{\rm Mn}$ corresponds to the Mn local spin-density.

The current-induced spin density has two contributions, $\mathbf{S} = \mathbf{S}^{\rm ext} + \mathbf{S}^{\rm int}$. The extrinsic contribution, $\mathbf{S}^{\rm ext}$,[2,3] arises from the non-equilibrium steady state distribution function of the carriers due to the interaction of the applied electric field and the spin-orbit coupling (SOC) carriers, *i.e.* predominantly independent of the magnetization and therefore of field-like form. However, there is another contribution not discussed theoretically before which is the focus of our study. This contribution arises from the electric-field induced polarization of the spins as they accelerate between scattering events, *i.e.* of purely intrinsic origin arising from the band structure of the system, which has the form, $\mathbf{S}^{\rm int} \propto \hat{M}\times\mathbf{a}(\mathbf{E})$, where $\mathbf{a}(\mathbf{E})$ is an in-plane function linear in the electric field that depends on the symmetry of the SOC responsible for the effect, Rashba or Dresselhaus, as discussed in the main text. This gives rise to an anti-damping torque, $\tau_{\rm anti-damp} \propto \hat{M}\times(\hat{M}\times\mathbf{a}(\mathbf{E}))$ and it is, in the case of (Ga,Mn)As, of the same order of magnitude as the extrinsic field-like SOT.

This current-induced non-equilibrium spin densities, $\mathbf{S}$, can be calculated by the linear Kubo response theory:[4]

$$\mathbf{S} = \frac{\hbar}{2\pi V}{\rm Re}\sum_{\mathbf{k},a,b}(\mathbf{s})_{ab}(e\mathbf{E}\cdot\mathbf{v})_{ba}[G^A_{\mathbf{k}a}G^R_{\mathbf{k}b} - G^R_{\mathbf{k}a}G^R_{\mathbf{k}b}], \tag{S10}$$

where the Green's functions $G^R_{\mathbf{k}a}(E)|_{E=E_F} \equiv G^R_{\mathbf{k}a} = 1/(E_F - E_{\mathbf{k}a} + i\Gamma)$, with the property $G^A = (G^R)^*$. The carrier states are labeled by momentum $\mathbf{k}$, band index a, and E_F is the Fermi energy. $\Gamma = \hbar/2\tau$ is the spectral broadening corresponding to a relaxation time τ.

Here the matrix elements of an operator $\hat{C}$ are $(\hat{C})_{ab} \equiv \langle \mathbf{k}a | \hat{C} | \mathbf{k}b \rangle$ or $(\hat{C})_a \equiv \langle \mathbf{k}a | \hat{C} | \mathbf{k}a \rangle$. The intra-band contributions in the above expressions correspond to the component already discussed before which gives rise to the field-like torque,[2–4] and the inter-band contribution is the one that gives rise to the intrinsic anti-damping SOT in analogy to the intrinsic SHE.

The expression for $\mathbf{S}^{\rm int}$ in the clean limit is given by

$$\mathbf{S}^{\rm int} = \frac{\hbar}{V} \sum_{\mathbf{k},a\neq b} \frac{{\rm Im}\left[(\mathbf{s})_{ab}(e\mathbf{E}\cdot\mathbf{v})_{ba}\right]}{(E_{\mathbf{k}a}-E_{\mathbf{k}b})^2}(f_{\mathbf{k}a}-f_{\mathbf{k}b}). \tag{S11}$$

Here $f_{\mathbf{k}a}$ are the Fermi-Dirac distribution functions corresponding to band energies $E_{\mathbf{k}a}$. In the presence of disorder, as it is the case for (Ga,Mn)As, the resulting expressions are approximated by

$$\begin{aligned}
\mathbf{S}^{\rm int} &= \mathbf{S}^{(1)} + \mathbf{S}^{(2)} \\
\mathbf{S}^{(1)} &= -\frac{1}{V} \sum_{\mathbf{k},a\neq b} 2{\rm Re}\left[(\boldsymbol{s})_{ab}(e\mathbf{E}\cdot\mathbf{v})_{ba}\right] \\
&\times \frac{\Gamma(E_{\mathbf{k}a}-E_{\mathbf{k}b})}{[(E_{\mathbf{k}a}-E_{\mathbf{k}b})^2+\Gamma^2]^2}(f_{\mathbf{k}a}-f_{\mathbf{k}b}) \\
\mathbf{S}^{(2)} &= -\frac{1}{V} \sum_{\mathbf{k},a\neq b} 2{\rm Im}\left[(\boldsymbol{s})_{ab}(e\mathbf{E}\cdot\mathbf{v})_{ba}\right] \\
&\times \frac{\Gamma^2-(E_{\mathbf{k}a}-E_{\mathbf{k}b})^2}{[(E_{\mathbf{k}a}-E_{\mathbf{k}b})^2+\Gamma^2]^2} f_{\mathbf{k}a}.
\end{aligned} \tag{S12}$$

Here we have ignored small numerical corrections due to the $G^R_{\mathbf{k}a}G^R_{\mathbf{k}b}$ terms which can be shown to formally vanish in a weak disorder situation and whose rapid oscillations can lead to numerical instabilities giving rise to systematic errors.

The hole-valence system is described by $H_{\rm GaAs} = H_{\rm KL} + H_{\rm strain}$, where the first term is the Kohn-Luttinger Hamiltonian and the second contains the strain effects. The four-band Kohn-Luttinger Hamiltonian in the hole-picture is

$$\begin{aligned}
H_{\rm KL} &= \frac{\hbar^2 k^2}{2m_0}\left(\gamma_1 + \frac{5}{2}\gamma 2\right)\mathbf{I}_4 - \frac{\hbar^2}{m_0}\gamma_3\left(\mathbf{k}\cdot\mathbf{J}\right)^2 \\
&+ \frac{\hbar^2}{m_0}(\gamma_3-\gamma_2)\left(k_x^2J_x^2 + k_y^2J_y^2 + k_z^2J_z^2\right).
\end{aligned} \tag{S13}$$

Here, $\mathbf{k}$ is the momentum of the holes, m_0 is the electron mass, $\gamma_1 = 6.98$, $\gamma_2 = 2.06$, and $\gamma_3 = 2.93$ are the Luttinger parameters, $\mathbf{I}_4$ is the 4×4 identity matrix and $\mathbf{J} = (J_x, J_y, J_z)$ are the 4×4 angular momentum matrices of the holes. Here the hole spin $\mathbf{s} = \boldsymbol{J}/3$, where $\boldsymbol{s}$ are the spin matrices for holes.[5]

The strain Hamiltonian in the hole-picture is

$$\begin{aligned} H_{\text{strain}} \;=\; & b\left[\left(J_x^2-\frac{\mathbf{J}^2}{3}\right)\epsilon_{xx}+\text{c.p.}\right] \\ & -C_4\left[J_x\left(\epsilon_{yy}-\epsilon_{zz}\right)k_x+\text{c.p.}\right] \\ & -C_5\left[\epsilon_{xy}(k_yJ_x-k_xJ_y)+\text{c.p.}\right], \end{aligned} \tag{S14}$$

where ϵ_{ij} is the strain tensor and $b=-1.7$ eV is the axial deformation potential. C_4 is the magnitude of the momentum-dependent Dresselhaus-symmetric strain term and C_5 is the magnitude of the Rashba-symmetric strain term. In our calculations, we use the value $C_4=10$ eVÅ calculated[6,7] from first principles for holes in (Ga,Mn)As and $C_5=C_4$. To the best of our knowledge, there is no measurement or calculation for the C_5 term in (Ga,Mn)As. In our calculations we set $\gamma_2=\gamma_3$ within the spherical approximation and for the parabolic approximation we set $\gamma_2=\gamma_3=0$ and take $\gamma_1=2$. The external electric field magnitude is set to $E=0.02$ mV/nm (from the experimental values), the disorder broadening to $\Gamma=25$ meV, and the strain to $\epsilon_{xx}=\epsilon_{yy}=-1.1\epsilon_{zz}=-0.3\%$ and $\epsilon_{xy}=-0.15\%$. The first term of the strain Hamiltonian is momentum independent. The other two terms are momentum-dependent and they are essential for the generation of SOT because they break the space inversion symmetry. The second term has a Dresselhaus symmetry and the third has a Rashba symmetry. As described in the experimental results, these symmetries are shared by the observed SOT. In this discussion we have neglected cubic Dresselhaus terms, allowed by the GaAs symmetry, since the experimentally observed SOTs vary linearly with strain.[3,8] We also note that in the above expressions we have ignored the Fermi-sea contribution corresponding to the Bastin formula of linear response since in this model it has been shown to vanish for the inter-band response.[9]

In Supplementary Fig. S3 we show the calculated z-component of the non-equilibrium spin polarization S_z in the 2D Rashba model as a function of Γ. The unit of energy is specified in the plot together with the relative size of the Fermi energy, the exchange splitting, and the spin-orbit splitting considered in these illustrative calculations. At small Γ the plotted numerical solution of Eq. (9) from the main text matches Eq. (5), as well as the expression $S_z=2g_{2D}JMs_{z,\mathbf{M}}$ obtained in the introductory part of the main text from the Bloch equations. We point out that the inter-band term of the Kubo formula (S10) giving rise to S_z is the only one which remains finite and non-zero at $\Gamma=0$. The inter and intra-band terms giving rise to the in-plane components of $\mathbf{S}$ are proportional to Γ and $1/\Gamma$,

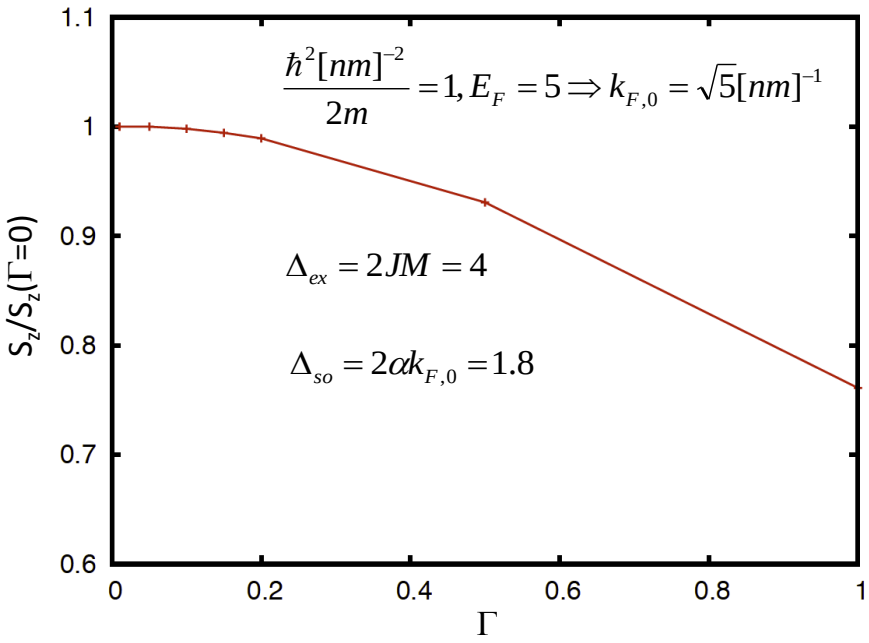

FIG. S3: Calculated z-component of the non-equilibrium spin polarization S_z in the 2D Rashba model as a function of Γ normalized to the S_z value at $\Gamma = 0$. The unit of energy is specified in the plot together with the relative size of the Fermi energy, the exchange splitting, and the spin-orbit splitting considered in the calculations.

respectively.[4]

Finally we remark that Eq. (9) of the main text describes the anti-damping SOT of the intrinsic origin within the relativistic quantum-mechanical transport formalism[4] well applicable to systems with strong spin-orbit coupling. This is in contrast to previously reported expressions for the extrinsic anti-damping SOT aimed to describe systems in the weak diffusion limit, which do not yield a finite non-zero SOT component in the absence of scattering.[10–13]

---

[1] Harder, M., Cao, Z. X., Gui, Y. S., Fan, X. L. & Hu, C. M. Analysis of the line shape of electrically detected ferromagnetic resonance. *Phys. Rev.* **B 84**, 054423 (2011).

[2] Manchon, A. & Zhang, S. Theory of spin torque due to spin-orbit coupling. *Phys. Rev.* **B 79**, 094422 (2009).

[3] Chernyshov, A. *et al.* Evidence for reversible control of magnetization in a ferromagnetic material by means of spin-orbit magnetic field. *Nature Phys.* **5**, 656 (2009). arXiv:0812.3160.

[4] Garate, I. & MacDonald, A. H. Influence of a transport current on magnetic anisotropy in gyrotropic ferromagnets. *Phys. Rev.* **B 80**, 134403 (2010). arXiv:0905.3856.

[5] Abolfath, M., Jungwirth, T., Brum, J. & MacDonald, A. H. Theory of magnetic anisotropy in $III_{1-x}Mn_xV$ ferromagnets. *Phys. Rev.* **B 63**, 054418 (2001). arXiv:cond-mat/0006093.

[6] Silver, M., Batty, W., Ghiti, A. & OReilly, E. P. Strain-induced valence-subband splitting in III-V semiconductors. *Physica* **B 46**, 6781 (1992).

[7] Stefanowicz, W. *et al.* Magnetic anisotropy of epitaxial (Ga,Mn)As on (113)a GaAs. *Phys. Rev.* **B 81**, 155203 (2010).

[8] Fang, D. *et al.* Spin-orbit driven ferromagnetic resonance: A nanoscale magnetic characterisation technique. *Nature Nanotech.* **6**, 413 (2011). arXiv:1012.2397.

[9] Kovalev, A. A., Sinova, J. & Tserkovnyak, Y. Anomalous hall effect in disordered multi-band metals. *Phys. Rev. Lett.* **105**, 036601 (2010).

[10] Kim, K.-W., Seo, S.-M., Ryu, J., Lee, K.-J. & Lee, H.-W. Magnetization dynamics induced by in-plane currents in ultrathin magnetic nanostructures with Rashba spin-orbit coupling. *Phys. Rev.* **B 85**, 180404(R) (2012).

[11] Pesin, D. A. & MacDonald, A. H. Quantum kinetic theory of current-induced torques in rashba ferromagnets. *Phys. Rev.* **B 86**, 014416 (2012).

[12] Wang, X. & Manchon, A. Diffusive spin dynamics in ferromagnetic thin films with a Rashba interaction. *Phys. Rev. Lett.* **108**, 117201 (2012).

[13] Manchon, A. Spin Hall effect versus Rashba torque: a diffusive approach (2012). arXiv:1204.4869.